Inorganic Chemistry

Article

pubs.acs.org/IC

Bulk and Molecular Compressibilities of Organic−Inorganic Hybrids $[(CH_3)_4N]_2MnX_4$ (X = Cl, Br); Role of Intermolecular Interactions

Jose Antonio Barreda-Argüeso,[†] Lucie Nataf,[†,§] Yamilet Rodríguez-Lazcano,[†] Fernando Aguado,[†] Jesús González,[†] Rafael Valiente,[‡] Fernando Rodríguez,*[,†] Heribert Wilhelm,[⊥] and Andrew P. Jephcoat[⊥]

[†]MALTA Consolider Team, Earth Science and Condensed Matter Physics Department (DCITIMAC), Facultad de Ciencias and [‡]MALTA Consolider Team, Applied Physics Department, University of Cantabria, 39005 Santander, Spain

[§]Synchrotron SOLEIL, L'Orme des Merisiers, St. Aubin BP48, 91192 Gif-sur-Yvette cedex, France

[⊥]Diamond Light Source Ltd., Chilton, Didcot, Oxfordshire, OX11 0DE, United Kingdom

Supporting Information

ABSTRACT: This work reports an X-ray diffraction, X-ray absorption, and Raman spectroscopy study of $[(CH_3)_4N]_2MnX_4$ (X = Cl, Br) under pressure. We show that both compounds share a similar phase diagram with pressure. A $P2_1/c$ monoclinic structure describes precisely the $[(CH_3)_4N]_2MnCl_4$ crystal in the 0.1−6 GPa range, prior to crystal decomposition and amorphization, while $[(CH_3)_4N]_2MnBr_4$ can be described by a *Pmcn* orthorhombic structure in its stability pressure range of 0−3 GPa. These materials are attractive systems for pressure studies since they are readily compressible through the weak interaction between organic/inorganic $[(CH_3)_4N^+/MnX_4^{2-}]$ tetrahedra through hydrogen bonds and contrast with the small compressibility of both tetrahedra. Here we determine the equation-of-state (EOS) of each crystal and compare it with the corresponding local EOS of the MnX_4^{2-} and $(CH_3)_4N^+$ tetrahedra, the compressibility of which is an order and 2 orders of magnitude smaller than the crystal compressibility, respectively, in both chloride and bromide. The variations of the Mn−Cl bond distance obtained by extended X-ray absorption fine structure and the frequency of the totally symmetric $\nu_1(A_1)$ Raman mode of $MnCl_4^{2-}$ with pressure in $[(CH_3)_4N]_2MnCl_4$ allowed us to determine the associated Grüneisen parameter (γ_{loc} = 1.15) and hence an accurate local EOS. On the basis of a local compressibility model, we obtained the Grüneisen parameters and corresponding variations of the intramolecular Mn−Br and C−N bond distances of $MnBr_4^{2-}$ (γ_{loc} = 1.45) and $(CH_3)_4N^+$ (γ_{loc} = 3.0) in $[(CH_3)_4N]_2MnBr_4$.

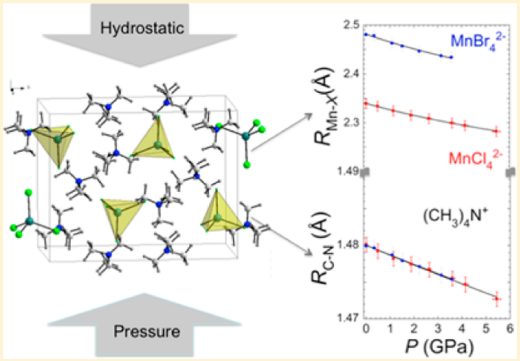

INTRODUCTION

Tetramethylammonium manganese tetrahalides $[(CH_3)_4N]_2MnX_4$ (X = Cl, Br) are organic−inorganic hybrid systems exhibiting relevant properties related to their ferroelectric and ferroelastic phases[1,2] and their highly efficient green photoluminescence.[3−7] Such properties are fully related to the inorganic MnX_4^{2-} and organic $(CH_3)_4N^+$ tetrahedra (T_d)[8] and their mutual interactions and thus can be strongly affected by an external pressure.[4−7] Furthermore, these systems are attractive for structural studies under pressure since they are expected to be easily compressible, and the interaction between organic/inorganic $[(CH_3)_4N^+/MnX_4^{2-}]$ tetrahedra strongly affects differently the crystal lattice and the tetrahedra, the cohesion of which is attained by hydrogen and covalence bonding, respectively.

In this work we investigate the variations of the crystal structure with pressure, from the orthorhombic structure, space group *Pmcn*,[9−11] aiming to correlate the structural changes in the lattice and around Mn^{2+}, establishing their different compressibility and how they eventually affect their properties. We studied the crystal equation of state (EOS), paying attention to the difference between the EOS for $[(CH_3)_4N]_2MnX_4$ and MnX_4^{2-}, which were determined through X-ray diffraction (XRD), X-ray absorption (XAS), and Raman spectroscopy under high-pressure conditions.

$[(CH_3)_4N]_2MnX_4$ crystals have been intensively investigated as model systems to elaborate a common pressure−temperature ($P-T$) phase diagram.[1,2,12,13] Each structural phase is related to the relative orientations of the organic/inorganic $[(CH_3)_4N^+/MnX_4^{2-}]$ tetrahedra emerging from their respective interactions through hydrogen bonds. Nevertheless no structural investigation of these materials under high-pressure conditions (P > 0.3 GPa) has been reported so far. In spite of the complexity and variety of structures exhibited by these compounds at ambient pressure and between low and room temperatures, for example, ferroelastic, incommensurate, ferroelectric, and paraelectric phases,[1,2,12] no other structures apart from the orthorhombic *Pmcn* have been reported at high temperature. Chemical pressure effects on the crystal structure

Received: August 3, 2014
Published: September 22, 2014

have been investigated through anion (X = Cl, Br) and cation (M = transition metal ion) substitution as a function of the crystal volume. In this way the replacement of Br for Cl and the substitution of M along the A_2MX_4 series, with Mn → Fe → Zn → Co, is known to be equivalent to a pressure increase in the common $P-T$ phase diagram.[1,2,12,13] It has been shown from dielectric measurements[1,2] that both crystals $[(CH_3)_4N]_2MnX_4$ experience a phase transition from orthorhombic *Pmcn* (Phase I) to monoclinic $P2_1/c$ (Phase V) at 0.3 GPa and 20 °C, according to this $P-T$ phase diagram.

The motivation to investigate crystal structure variation with pressure in $[(CH_3)_4N]_2MnX_4$ is twofold. First, the compressibility of these materials (related to the interactions between organic−inorganic tetrahedra through hydrogen bonds) is expected to be higher than the local compressibility of the covalently bonded tetrahedra. The comparison between bulk and local compressibilities provides crucial structural information to unveil the stability of both organic/inorganic tetrahedra against compression. Second, these pressure experiments allow us to reduce the interatomic distance between MnX_4^{2-} units affecting the superexchange interaction, thus magnetism and photoluminescence.[5,7]

EXPERIMENTAL SECTION

Single crystals of $[(CH_3)_4N]_2MnCl_4$ and $[(CH_3)_4N]_2MnBr_4$ were grown by slow evaporation at 5 °C from HCl (or HBr) acidic solution (pH ≈ 2−3) containing a 2:1 stoichiometric ratio of the tetramethylammonium halide $[(CH_3)_4NX]$ and the corresponding metallic halide MnX_2 (ref 8). Their orthorhombic crystal structure, space group *Pmcn*, at ambient conditions was checked by XRD using a Bruker D8 Advance diffractometer and a polarizing microscope. The obtained lattice parameters are a = 9.23 Å; b = 15.93 Å; and c = 12.63 Å for $[(CH_3)_4N]_2MnBr_4$; and a = 9.07 Å; b = 15.66 Å, c = 12.33 Å for $[(CH_3)_4N]_2MnCl_4$ in good agreement with the literature.[6,8] The Mn^{2+} is tetrahedraly coordinated with bond distance of R_{Mn-Br} = 2.48 Å and R_{Mn-Cl} = 2.34 Å. The crystal structure showing the $(CH_3)_4N^+$ and MnX_4^{2-} tetrahedra is depicted in Figure 1. Note that the closest Mn−Mn distances are 8.18 Å[9] and 8.11 Å[11] for the bromide and chloride, respectively.

Unpolarized micro-Raman scattering measurements were performed in a triple monochromator Horiba−Jobin−Yvon T64000 spectrometer in subtractive mode backscattering configuration, equipped with a liquid nitrogen-cooled charge-coupled device detector. To avoid the strong green photoluminescence, the spectra were obtained with the 647 nm lines of an Ar^+-Kr^+ laser. The beam was focused on the sample with a 20× objective for micro-Raman, and the laser power was kept below 5 mW to avoid heating effects. The laser spot was 20 μm in diameter, and the spectral resolution was better than 1 cm^{-1}. The Raman technique was used to check the sample structure through the characteristic first-order stretching local modes of the $(CH_3)_4N^+$ and MnX_4^{2-} tetrahedra. In particular, we study the pressure dependence of the totally symmetric A_1 frequencies associated with the Mn−X and C−N stretching modes, the values of which at ambient conditions are 253 cm^{-1} for $MnCl_4^{2-}$, 156 cm^{-1} for $MnBr_4^{2-}$, and 750 cm^{-1} for $(CH_3)_4N^+$. These values agree with those given elsewhere.[14−17]

XRD experiments under high-pressure conditions were performed in the diffraction setup of the I15 Extreme Conditions beam station at DIAMOND. Powder XRD experiments were carried out using wavelength of λ = 0.4387 Å and the MAR345 image plate detector. A novel Merril−Basset-type diamond anvil cell (DAC) developed by the MALTA Consolider consortium (Spain) was employed for pressure experiments in the 0−6 GPa range. The DAC was loaded with powders of either $[(CH_3)_4N]_2MnCl_4$ or $[(CH_3)_4N]_2MnBr_4$, ruby spheres (<10 μm diameter), and silicone oil (Dow Corning 200 fluid 300 000 cst) as pressure-transmitting medium to prevent sample moisture. We performed joint XRD and in situ photoluminescence spectroscopy on powders of $[(CH_3)_4N]_2MnCl_4$ and $[(CH_3)_4N]_2MnBr_4$ under high pressure in the 0−6 GPa and 0−4 GPa range, respectively, to check the green emission from MnX_4^{2-}. Processing of diffraction images was performed with the FIT2D software,[18] whereas TOPAS was used for structural (Pawley-type) analysis.

X-ray absorption measurements under pressure were obtained at the ODE beamline at SOLEIL synchrotron using energy dispersive setup[19] with pink beam around the Mn K-edge (E = 6.539 keV) and were carried out on a membrane-type DAC. 150 μm thick stainless steel gaskets were preindented, and suitable 200 μm diameter holes were perforated, with a BETSA motorized electrical discharge machine. The DAC was loaded with a powder and ruby microspheres (<10 μm diameter) using silicone oil as pressure-transmitting medium. Unfortunately, the inorganic units of he sample interact with the polychromatic beam (around the Mn K-edge) as observed through the modifications in XAS when sample was irradiated for more than few minutes. Because of this, XAS spectra were acquired in a short time (less than 1 min) to prevent radiation damage of the sample (see Supporting Information).

In all experiments, pressure was measured through the ruby photoluminescence.[20,21]

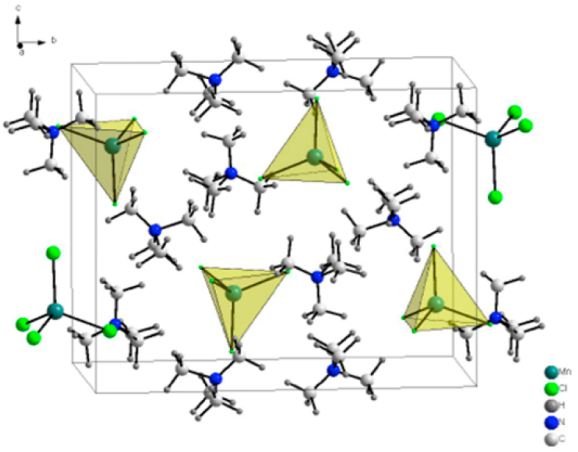

Figure 1. Unit cell of $[(CH_3)_4N]_2MnX_4$ (X = Cl, Br) at ambient conditions: orthorhombic, space group *Pmcn*. Note the independent character of the MnX_4^{2-} (green) and $(CH_3)_4N^+$ (N blue; C,H gray) tetrahedra. The closest N−Mn and Mn−Mn distances in $[(CH_3)_4N]_2MnCl_4$ are 5.0 and 8.2 Å, respectively.

RESULTS AND DISCUSSION

1. Pressure Dependence of the Crystal Structure of $[(CH_3)_4N]_2MnBr_4$ and $[(CH_3)_4N]_2MnCl_4$. The two investigated crystals $[(CH_3)_4N]_2MnX_4$ (X = Br, Cl) show a common *Pmcn* orthorhombic structure at ambient conditions consisting of MnX_4^{2-} and $(CH_3)_4N^+$ tetrahedra located in the unit cell as indicated in Figure 1. Their XRD patterns as a function of pressure are shown in Figure 2. Above 0.3 GPa, XRD patterns can be indexed on the basis of a monoclinic structure, space group $P2_1/c$ (Phase V, $c = c_0$),[2] in the whole pressure range. However, in $[(CH_3)_4N]_2MnBr_4$ no significant deviation of the angle β from 90° is observed; thus, a *Pmcn* space group can be used to describe XRD patterns up to the crystal decomposition and amorphization, which starts at about 4 GPa (6 GPa in $[(CH_3)_4N]_2MnCl_4$).[7] Photoluminescence studies indicate that these high-pressure amorphized phases involve a change of coordination from MnX_4^{2-} to MnX_6^{4-} as shown through the characteristic luminescence color changing from green (T_d) to red (O_h) and thus stressing the suitability of optical spectroscopy as an efficient local probe to explore pressure-

dx.doi.org/10.1021/ic501854g | Inorg. Chem. 2014, 53, 10708−10715

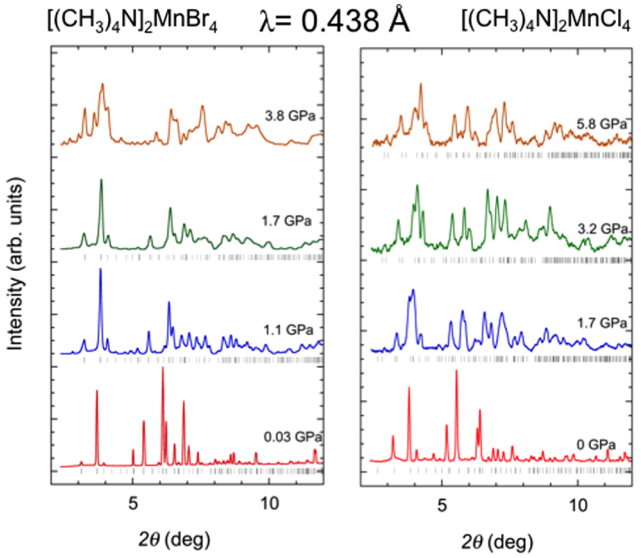

Figure 2. XRD patterns of $[(CH_3)_4N]_2MnBr_4$ and of $[(CH_3)_4N]_2MnCl_4$ as a function of pressure. Crystal structure: orthorhombic *Pmcn* structure at ambient pressure and monoclinic $P2_1/c$ above 0.1 GPa in the case of $[(CH_3)_4N]_2MnCl_4$.

induced aggregation phenomena in $[(CH_3)_4N]_2MnX_4$ (ref 7). Structural data indicate that the distance between closest MnX_4^{2-} tetrahedra (R_{Mn-Mn} = 8.1 Å)[9,11] is twice as large as the Mn−Mn distance attained in 6-fold-coordinated compounds. In these compounds the Mn−Mn separation is dimensionality-dependent and has values of R_{Mn-Mn} = 3.25 and 3.38 Å for the one-dimensional $[(CH_3)_4N]MnX_3$ for X = Cl and Br, respectively,[22,23] R_{Mn-Mn} = 5.05 and 5.37 Å in the two-dimensional Rb_2MnX_4 (X = Cl, Br),[24,25] or R_{Mn-Mn} = 5.04 Å in the three-dimensional NH_4MnCl_3 (ref 26). It means that volume reductions of about 50% would approach MnX_4^{2-} to distances comparable to those attained in concentrated compounds; hence, important aggregation phenomena would be expected in $[(CH_3)_4N]_2MnX_4$ at pressures comparable to the bulk modulus. The XRD patterns at 3.8 GPa in $[(CH_3)_4N]_2MnBr_4$ and 5.8 GPa in $[(CH_3)_4N]_2MnCl_4$ give clear evidence of both crystal structure transformation and partial amorphization (Figure 2), thus confirming this view.

Table 1 collects the lattice parameters and cell volume as a function of pressure derived from XRD data for the two $[(CH_3)_4N]_2MnX_4$ compounds, either in the ambient pressure *Pmcn* structure or in the high-pressure $P2_1/c$ structure. A Murnaghan EOS[27] was fitted to the experimental data $V(P)$, shown in Figure 3.

$$V(P) = V_0\left(1 + \frac{B'P}{B}\right)^{-1/B'} \quad (1)$$

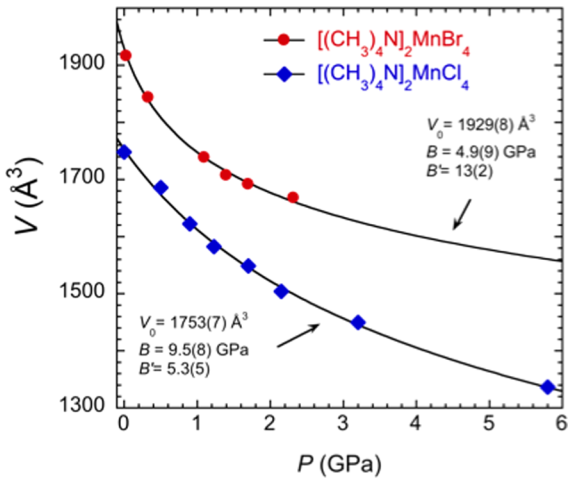

Figure 3. Pressure dependence of the cell volume $V(P)$ derived from X-ray diffraction data (see Table 1). The curves correspond to Murnaghan's equations of state.

where V_0, B, and B' are the ambient pressure cell volume, the bulk modulus and its pressure derivative, respectively. The fitting gives V_0 = 1753(4) Å^3, B = 9.5(8) GPa, and B' = 5 for $[(CH_3)_4N]_2MnCl_4$; it gives V_0 = 1930(4) Å^3, B = 4.9(6) GPa, and B' = 13 for $[(CH_3)_4N]_2MnBr_4$. It is worth noting that the bulk modulus increases twice on passing from bromide to chloride; however, its pressure derivative is bigger for bromides indicating that in these compounds the intertetrahedra interactions by hydrogen bonds, although weak in the bromide at low pressure, become stronger than chloride as pressure increases.

2. Variation of the Mn−Cl Distance with Pressure in $[(CH_3)_4N]_2MnCl_4$ by Means of Extended X-ray Absorption Fine Structure. Figure 4 shows the X-ray absorption spectra, $\mu(E)$, of $[(CH_3)_4N]_2MnCl_4$ around the Mn K edge, E = 6.539 keV, as a function of pressure, and the corresponding Fourier transform (FT) spectra, $\chi(R)$. Both spectra clearly

Table 1. Lattice Parameters and Cell Volume of $[(CH_3)_4N]_2MnX_4$ (X = Cl, Br) as a Function of Pressure

$[(CH_3)_4N]_2MnCl_4$								
	10^{-4} GPa	0.5 GPa	0.9 GPa	1.2 GPa	1.7 GPa	2.2 GPa	3.2 GPa	5.8 GPa
a (Å)	9.046	8.968	8.863	8.814	8.770	8.712	8.643	8.458
b (Å)	15.669	15.377	15.122	14.946	14.800	14.591	14.331	13.838
c (Å)	12.333	12.223	12.105	12.013	11.936	11.837	11.712	11.434
β (deg)	90	90	90	90	88.3	88.5	87.8	86.9
V (Å^3)	1748.1	1685.7	1622.3	1582.4	1548.5	1504.2	1449.5	1336.4
$[(CH_3)_4N]_2MnBr_4$								
	0.03 GPa	0.17 GPa	0.33 GPa	1.1 GPa	1.4 GPa	1.7 GPa		
a (Å)	9.293	9.292	9.176	9.062	9.031	8.850		
b (Å)	16.185	16.203	15.925	15.527	15.439	15.544		
c (Å)	12.740	12.745	12.616	12.356	12.244	12.295		
V (Å^3)	1916.2	1918.9	1843.5	1738.6	1707.2	1691.4		

dx.doi.org/10.1021/ic501854g | Inorg. Chem. 2014, 53, 10708−10715

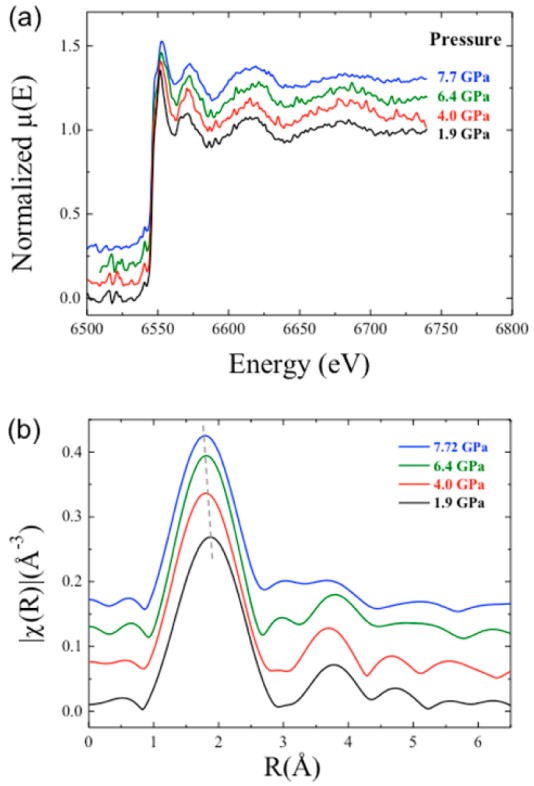

Figure 4. (a) Variation of the X-ray absorption spectrum, $\mu(E)$, around the Mn K-edge of $[(CH_3)_4N]_2MnCl_4$ in the 0−8 GPa range. (b) FT-EXAFS, $\chi(R)$, from Mn K-edge as a function of pressure.

show that Mn^{2+} is tetrahedrally coordinated in the 0−6 GPa range prior to amorphization.[7] It is worth noting that XAS experiments were done with irradiation doses on the sample below the damage threshold (see Supporting Information). The first peak in $\chi(R)$ shifts to lower R values with pressure, indicating a decrease of the tetrahedral Mn−Cl bond length with pressure. Extended X-ray absorption fine structure (EXAFS) analysis using the Demeter package[28] reveals that the spectra can be accounted for on the basis of a $MnCl_4^{2-}$ (T_d symmetry) with one Mn−Cl distance, R_{Mn-Cl}. Its variation with pressure is shown in Figure 5. Although the error of R_{Mn-Cl} is $\Delta R_{Mn-Cl} = \pm 0.02$ Å, $R_{Mn-Cl}(P)$ data show a linear dependence

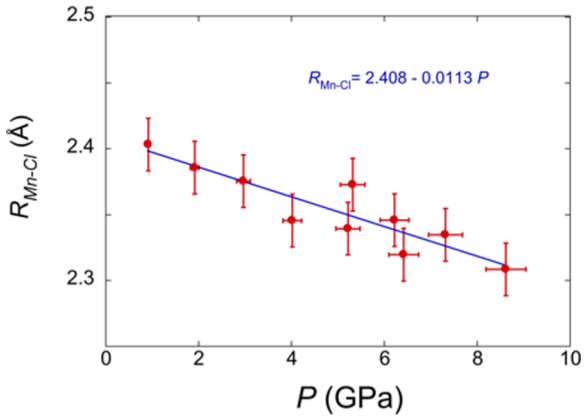

Figure 5. Variation of the EXAFS-derived Mn−Cl distance with pressure in $[(CH_3)_4N]_2MnCl_4$. Statistical errors are associated with the different loading required for each pressure point.

with pressure in the 0−8 GPa range, whose least-squares fitting provides a linear equation, $R_{Mn-Cl}(P) = 2.408 + 11.3 \times 10^{-3}P$ (units in Å and GPa, respectively), with a regression coefficient better than $R = 0.91$. From these experimental data, we can determine the local bulk modulus of the $MnCl_4^{2-}$ tetrahedron, B_{loc}, through the compressibility by the equation

$$\kappa_{loc} = B_{loc}^{-1} = \frac{3}{R_{Mn-Cl}} \frac{\partial R_{Mn-Cl}}{\partial P} \quad (2)$$

The observed linear dependence of $R_{Mn-Cl}(P)$ leads to $B_{loc} = 71(3)$ GPa. This value is an order of magnitude higher than the crystal bulk modulus of $[(CH_3)_4N]_2MnCl_4$ ($B_0 = 9.5(8)$ GPa), thus indicating that the inorganic tetrahedron is tougher than the crystal as consequence of the weaker cohesion provided by intermolecular hydrogen bonds in comparison to the stiff Mn−Cl covalent bonds of the tetrahedron. The so-obtained B_{loc} value is similar to that estimated from optical spectroscopy, $B_{loc}(opt) = 87$ GPa, on the assumption that T_d crystal-field splitting, Δ, between t_2 and e Mn^{2+} one-electron levels increases with pressure as $\Delta = kR_{Mn-Cl}^{-5}$ (ref 7). In view of present EXAFS data the optical spectroscopy-derived $B_{loc}(opt)$ can be reconciled with the EXAFS-derived B_{loc} on the assumption of an R_{Mn-Cl} dependence of Δ proportional to R_{Mn-Cl}^{-n} with an exponent $n = 4.1$. This is the first experimental determination of this exponent for a transition-metal ion complex with T_d symmetry and reflects the deviation from the exponent $n = 5$, usually found in more ionic bond systems like octahedral chlorides and most fluorides and oxides.[7,29,30]

Unfortunately, we were unable to obtain suitable XAS of $[(CH_3)_4N]_2MnBr_4$ under high-pressure conditions in DAC because EXAFS oscillations were weak and smoothed preventing any reliable structural analysis beyond ambient conditions. However, as we will see in the next section, we estimated the local bulk modulus for $MnBr_4^{2-}$ from Raman spectroscopy, obtaining $B_{loc} = 58$ GPa. This value is similar to that obtained by optical spectroscopy, $B_{loc}(opt) = 52$ GPa, using $\Delta = kR_{Mn-Br}^{-5}$ (ref 7). The EXAFS-derived local bulk modulus is consistent with the optical one assuming an exponent $n = 5.6$, which significantly deviates from $n = 5$, thus clearly showing strong covalency effects.

3. Variation of the Raman A_1 Mode with Pressure: Local Grüneisen Parameter and Equation-of-State.

Figure 6 shows the unpolarized Raman spectra of the two $[(CH_3)_4N]_2MnX_4$ compounds at ambient conditions. The spectra consist of several peaks, which can be easily identified with Raman active internal modes of the MnX_4^{2-} and $(CH_3)_4N^+$ tetrahedra.[14−17] The modes of the inorganic tetrahedra are located in the 70−350 cm^{-1} range, whereas the modes of interest of the $(CH_3)_4N^+$ ions are observed in the 350−1000 cm^{-1} range.

The comparison of the two spectra allows us to distinguish between $MnCl_4^{2-}$ (or $MnBr_4^{2-}$) modes and those of $(CH_3)_4N^+$, the latter ones appearing at about the same frequency in both spectra. Table 2 collects the ambient pressure frequencies of the more representative Raman active modes. In particular, the two E and T_2 bending modes and the two A_1 and T_2 stretching modes of the inorganic tetrahedra MnX_4^{2-} appear at 116 cm^{-1} (ν_4) for the T_2 bending mode and at 255 cm^{-1} (ν_1) for the A_1 stretching mode in $[(CH_3)_4N]_2MnCl_4$. In $[(CH_3)_4N]_2MnBr_4$ frequencies are 77 cm^{-1} (ν_4) for the T_2 bending mode and 158 cm^{-1} (ν_1) for the A_1 stretching mode. These frequency and mode assignments are in agreement with values given for

dx.doi.org/10.1021/ic501854g | Inorg. Chem. 2014, 53, 10708−10715

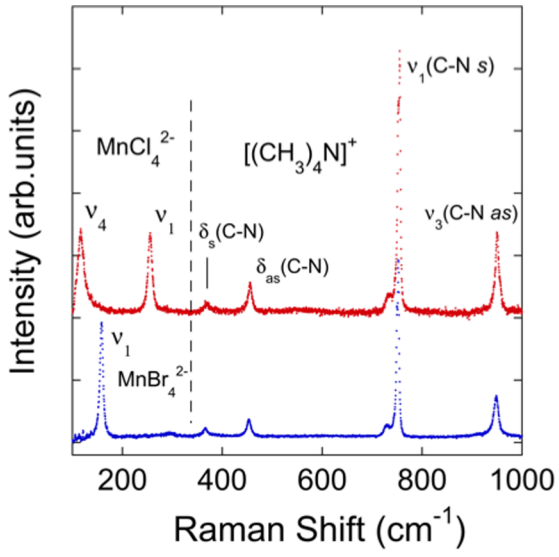

Figure 6. Raman spectra of $[(CH_3)_4N]_2MnCl_4$ and $[(CH_3)_4N]_2MnBr_4$ at ambient conditions. Raman modes (T_d symmetry) and observed vibrational frequencies are given in Table 2.

MnX_4^{2-} complexes in solution,[14] but Raman bending (ν_2) and stretching (ν_3) modes for MnX_4^{2-}, both of T_2 symmetry, are not observed in present experiments. Interestingly, the observation of the totally symmetric A_1 stretching mode for $MnCl_4^{2-}$ and $MnBr_4^{2-}$ together with the equivalent stretching mode of the $(CH_3)_4N^+$ ($\nu_1 = 750\ cm^{-1}$) is noteworthy. Their frequency and corresponding pressure shift are both proportional to the Mn−X and N−CH_3 bond lengths, respectively, through the corresponding local Grüneisen parameter, defined as

$$\gamma_{loc}(A_1) = -\left(\frac{\partial \ln[\nu_1(A_1)]}{\partial \ln[V_{loc}]}\right) = \frac{-1}{3}\left(\frac{\partial \ln[\nu_1(A_1)]}{\partial \ln[R_{loc}]}\right) \quad (3)$$

Here $\nu_1(A_1)$ is the vibrational mode frequency, and V_{loc} and R_{loc} are the local volume and bond length, respectively, in the corresponding organic/inorganic tetrahedron. Note that the thermodynamic definition of parameters B and γ involves the crystal volume, not local volumes. The parameter $\gamma_{loc}(A_1)$, together with the isothermal local bulk modulus of the tetrahedron from eq 4, allows us to relate these two parameters with the pressure shifts:

$$B_{loc} = -V_{loc}\left(\frac{\partial P}{\partial V_{loc}}\right)_T = -\frac{1}{3}R_{loc}\left(\frac{\partial P}{\partial R_{loc}}\right)_T \quad (4)$$

$$\frac{1}{\nu_1(A_1)}\left(\frac{\partial \nu_1(A_1)}{\partial P}\right)_{P\to 0} = \frac{\gamma_{loc}(A_1)}{B_{loc}} = \frac{\gamma(A_1)}{B} \quad (5)$$

In the second and third terms of eq 5, the frequency shift scales to the local volume of the tetrahedron and the crystal volume, respectively, B and $\gamma(A_1)$ being the bulk modulus and the Grüneisen parameter of the A_1 mode, respectively.

The variation of the stretching A_1 mode with pressure $\nu_1(P)$ is shown in Figure 7 together with the corresponding least-squares linear fit equations. The blueshift observed in the stretching A_1 mode in $MnCl_4^{2-}$, $MnBr_4^{2-}$, and $(CH_3)_4N^+$ clearly indicates that the tetrahedral bond distances Mn−Cl, Mn−Br, and N−CH_3 decrease with pressure. From these variations, we can extract information on both (local and bulk) Grüneisen parameters through the corresponding bulk moduli. The

Table 2. Vibrational Frequencies, ν, of the Raman Modes Corresponding to $[(CH_3)_4N]_2MnCl_4$ and $[(CH_3)_4N]_2MnBr_4$ at Ambient Conditions

crystal	$[(CH_3)_4N]_2MnCl_4$						$[(CH_3)_4N]_2MnBr_4$					
molecular ion	$MnCl_4^{2-}$		$(CH_3)_4N^+$				$MnBr_4^{2-}$		$(CH_3)_4N^+$			
T_d mode	$\nu_4(T_2)^a$	$\nu_1(A_1)^a$	$\nu_2(\delta_s(E))^a$	$\nu_4(\delta_{as}(T_2))^a$	$\nu_1(A_1)^a$	$\nu_3(T_2)^a$	$\nu_4(T_2)^a$	$\nu_1(A_1)^a$	$\nu_2(\delta_s(E))^a$	$\nu_4(\delta_{as}(T_2))^a$	$\nu_1(A_1)^a$	$\nu_3(T_2)^a$
ν (cm^{-1}) ($P = 0$)	116.2	255.3	368	455	753.3	950	76.7	158.2	366	454	752	948
$(\partial\nu/\partial P)$(cm^{-1}/GPa)		5.2			6.1			3.2			6.0	
ν_0 (cm^{-1})		253.9			751.7			161.7			751.6	
γ		0.19(2)			0.077(8)			0.10(1)			0.039(8)	
γ_{loc}		1.45(15)			3.0(3)			1.15			3.0(3)	
B(GPa)			9.5(8) with $B' = 5$						4.9(6) with $B' = 13$			
B_{loc}(GPa) ($B' = 0$)	71(3)			370(20)			58(3)			370(20)		
B_{loc}(GPa) ($B' = 7$)	57(2)			360(20)			48(3)			360(20)		

[a]High-frequency modes at Γ ($k = 0$) correspond to internal modes of the tetrahedron and are labelled according to the T_d symmetry irreducible representations: ν_1 and ν_2 are the stretching symmetric (s) A_1 and antisymmetric (as) T_2 modes, respectively, and ν_3 and ν_4 are the low-frequency bending E and T_2 modes, respectively, of the MnX_4^{2-} and $(CH_3)_4N^+$ tetrahedra.[14,16,17] The pressure derivative and zero-pressure frequency, ν_0, are obtained by least-square fitting of the linear pressure dependence of $\nu_1(P)$. The bulk and local Grüneisen parameters, γ and γ_{loc}, respectively, are obtained through eq 5 using the bulk modulus B and the local bulk modulus B_{loc}, respectively. B and B' were determined by fitting $V(P)$ to a Murnaghan EOS, and B_{loc} was determined for pressure derivative values $B' = 0$ and 7.

dx.doi.org/10.1021/ic501854g | Inorg. Chem. 2014, 53, 10708−10715

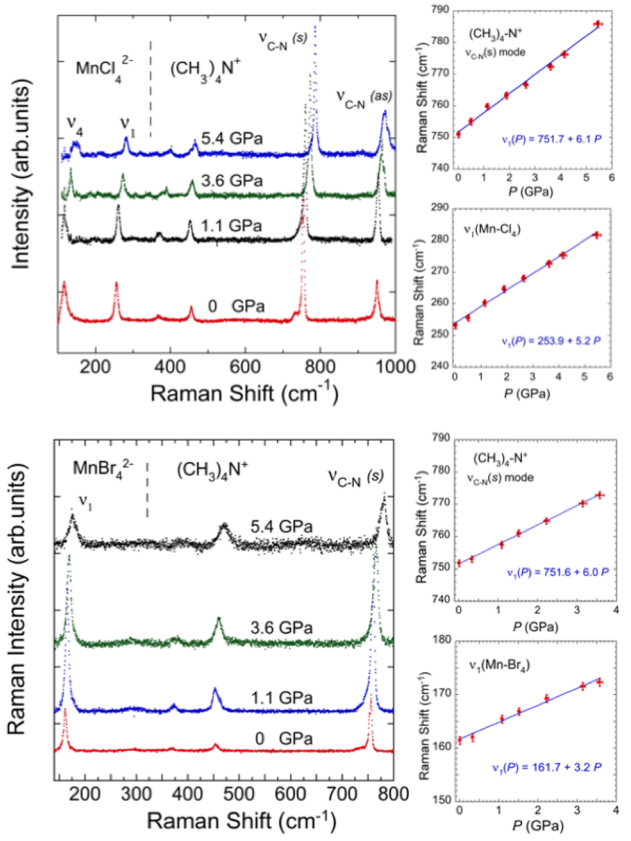

Figure 7. Raman spectra of $[(CH_3)_4N]_2MnCl_4$ and $[(CH_3)_4N]_2MnBr_4$ at selected pressures. Pressure dependences of the stretching A_1 frequency ν_1 for $MnCl_4^{2-}$, $MnBr_4^{2-}$, and $(CH_3)_4N^+$ are indicated rightside.

pressure dependence of the bond length can be obtained through the A_1 frequency shift if the local Grüneisen parameter is known. Note that this information can be obtained through the stretching A_1 mode since the associated normal coordinate (Q_1) is directly related to variations of the Mn−X or N−CH_3 bond lengths: $Q_1 \equiv \delta R_{loc}$.

Table 2 includes pressure shifts of the Raman frequencies for the stretching A_1 mode of the tetrahedra, the local bulk moduli and compressibilities, as well as the bulk and local Grüneisen parameters in $[(CH_3)_4N]_2MnX_4$. The local Grüneisen parameters for $MnCl_4^{2-}$ and $MnBr_4^{2-}$ are $\gamma_{loc}(A_1) = 1.45$ and 1.15, respectively. The former value was directly obtained from the variation of the 255 cm^{-1} mode (A_1) with pressure, $[\partial\nu_1(A_1)/\partial P] = 5.2$ cm^{-1}/GPa, and the local bulk modulus was derived by EXAFS through eq 4: $B_{loc} = 71(3)$ GPa (Figure 5). Although we could not obtain information on $R_{Mn-Br}(P)$ by EXAFS in $[(CH_3)_4N]_2MnBr_4$, it is possible to estimate B_{loc} for $MnBr_4^{2-}$ by comparing pressure dependences of $\nu_1(P)$ in both systems $[(CH_3)_4N]_2MnX_4$ (X = Cl, Br).

For a given MnX_4^{2-} tetrahedron the external force acting on the Mn−X bond at P is proportional to the effective tetrahedron surface: $F^{ext}_{Mn-X} = S_{eff} \times P = R_{loc}^2 \times P$. This external force reduces the equilibrium bond distance to an extent given by the force constant of the Mn−X bond.

$$F^{ext}_{Mn-X} = -K \times \delta R_{loc} = -\mu_X \times \nu_1^2 \times \delta R_{Mn-X} \quad (6)$$

where μ_X is the X (Cl or Br) mass, ν_1 the mode frequency, and $\delta R_{Mn-X} = R_{Mn-X}(P) - R_{Mn-X}(0)$, the Mn−X bond distance variation at P. By considering that $P = (F_{ext}/S_{eff})$ and combining eqs 4−6 for $MnCl_4^{2-}$ and $MnBr_4^{2-}$, we obtain

$$\frac{B_{loc}(MnBr_4^{2-})}{B_{loc}(MnCl_4^{2-})} = \frac{\frac{\delta R_{Mn-Cl}}{R_{Mn-Cl}}}{\frac{\delta R_{Mn-Br}}{R_{Mn-Br}}} = \frac{\mu_{Br} \times \nu_{Br}^2 \times R_{Mn-Cl}}{\mu_{Cl} \times \nu_{Cl}^2 \times R_{Mn-Br}} \quad (7)$$

Taking $(\mu_{Br}/\mu_{Cl}) = (80/35.5) = 2.25$, $\nu_{Br}^2/\nu_{Cl}^2 = (158/255)^2 = 0.384$, and $R_{Mn-Cl}/R_{Mn-Br} = (2.34/2.48) = 0.943$, we deduce $B_{loc}(MnBr_4^{2-}) = 0.816 \times B_{loc}(MnCl_4^{2-}) = 58(3)$ GPa. The local Grüneisen parameter for $\nu_1(A_1)$ in $MnBr_4^{2-}$ is then $\gamma_{loc}(A_1) = 1.15$, using eq 5 and $[1/(\nu_1(A_1))][\partial\nu_1(A_1)/\partial P]_{Mn-Br} = 0.0198$ GPa^{-1} (Figure 7).

A similar deduction for the totally symmetric N−CH_3 stretching vibration of the $(CH_3)_4N^+$ tetrahedron yields

$$\frac{B_{loc}(N(CH_3)_4^+)}{B_{loc}(MnCl_4^{2-})} = \frac{\frac{\delta R_{Mn-Cl}}{R_{Mn-Cl}}}{\frac{\delta R_{N-CH_3}}{R_{N-CH_3}}} = \frac{\mu_{CH_3} \times \nu_{N-CH_3}^2 \times R_{Mn-Cl}}{\mu_{Cl} \times \nu_{Cl}^2 \times R_{N-CH_3}} \quad (8)$$

Taking $(\mu_{CH_3}/\mu_{Cl}) = (15/35.5) = 0.42$, $\nu_{N-CH_3}^2/\nu_{Cl}^2 = (752/255)^2 = 8.70$, and $R_{Mn-Cl}/R_{N-CH_3} = (2.34/1.66) = 1.41$, we deduce $B_{loc}((CH_3)_4N^+) = 5.2 \times B_{loc}(MnCl_4^{2-}) = 370(20)$ GPa. Taking $[1/\nu_1(A_1)][\partial\nu_1(A_1)/\partial P]_{C-N} = 0.0080(2)$ GPa^{-1} for the N−$(CH_3)_4$ mode (A_1) in $[(CH_3)_4N]_2MnCl_4$ and $[(CH_3)_4N]_2MnBr_4$ (Figure 7), we obtain $\gamma_{loc}(A_1) = 3.0(0.3)$ from eq 5. This result is noteworthy since the pressure-induced variation of the intramolecular C−N distance is in many cases difficult to extract from XRD data of organic/inorganic hybrid complex systems. Nevertheless it can be derived from $\nu_1(A_1)$, given that this frequency is very sensitive to pressure even for moderate pressure ($P < 10$ GPa).

Figure 8 shows the pressure dependence of $R_{Mn-X}(P)$ and $R_{C-N}(P)$ derived from the corresponding $\nu_1(A_1)$ and $\gamma_{loc}(A_1)$ values.

Such pressure dependences are seen to be quasi-linear for $MnBr_4^{2-}$ and $(CH_3)_4N^+$ but deviate significantly from linearity for $MnCl_4^{2-}$. The fit of $R_{Mn-Cl}(P)$ using Murnaghan EOS provides values of $B = 58$ GPa and $B' = 7(1)$, which contrasts with the initial value $B = 71$ GPa obtained on the assumption that $B' = 0$. It must be underlined that these deviations are inherent to the Murnagahn EOS since suitable fitting of a quasi-linear variation of $R(P)$ are attained for different choices of B and B' parameters (coupled parameters). Table 2 collects the local EOS for each molecule, the two bulk modulus data corresponding to $B' = 0$ and 7, and associated compressibilities. Note that EOS fitting with $B' = 0$ provides identical bulk moduli as those obtained from linear approximation.

The analysis of the isothermal compressibility $\kappa = 1/B$ in terms of volume partitioning confirms the model consistency. Furthermore, this model is ideal for those molecular crystals consisting of organic/inorganic tetrahedral ions linked by Coulomb and hydrogen-bonding interactions and, in general, for molecular systems where inter- and intramolecular interactions are very different. According to experimental values of the bulk (crystal) and local compressibilities of tetrahedra (Table 2), we conclude that is mainly governed by intermolecular interactions rather than molecular compressibility. This behavior is due to the tight ionic−convalent Mn−X bonds and the stronger covalent C−N bond, in comparison to the weaker hydrogen-like intermolecular interactions, making tetrahedra quasi-rigid molecules upon crystal compression in

dx.doi.org/10.1021/ic501854g | Inorg. Chem. 2014, 53, 10708−10715

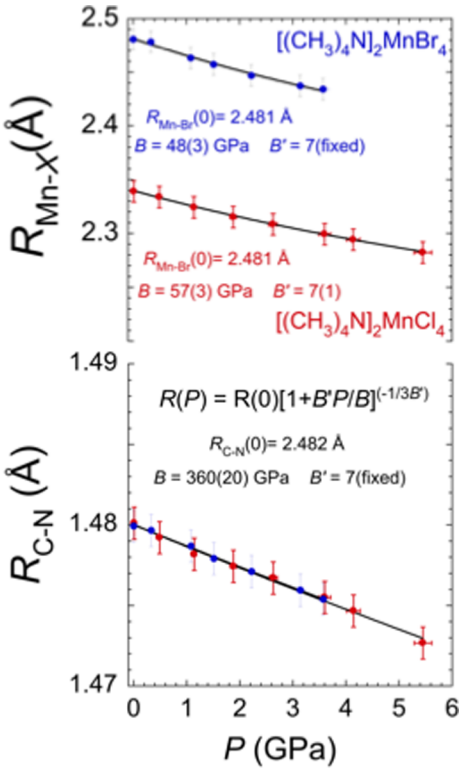

Figure 8. Variation of the Mn−X (X = Cl, Br) and C−N bond lengths with pressure in $[(CH_3)_4N]_2MnCl_4$ (red points) and $[(CH_3)_4N]_2MnBr_4$ (blue points).

the explored pressure range ($P < B_0$). In general, crystal compressibility can be partitioned as follows:[31,32]

$$\kappa = \frac{1}{B} = \frac{1}{V}\left(\frac{\partial V}{\partial P}\right)_T = \sum_i \frac{V_i}{V}\frac{1}{V_i}\left(\frac{\partial V_i}{\partial P}\right)_T = \sum_i \alpha_i \kappa_i \quad (9)$$

where the volume V is divided in N partitions, each having a volume of V_i. $\alpha_i = (V_i/V)$ and $\kappa_i = (1/V_i)((\partial V_i)/(\partial P))_T$ are the volume fraction and local isothermal compressibility of molecule i and intermolecular space in the $[(CH_3)_4N]_2MnX_4$ unit cell, respectively. The summation extends over eight $(CH_3)_4N^+$, four MnX_4^{2-}, and the remainder intermolecular space in the unit cell. Then we get

$$\kappa([(CH_3)_4N]_2MnX_4) = \frac{\alpha_{N(CH_3)_4}}{V_{N(CH_3)_4}}\left(\frac{\partial V_{N(CH_3)_4}}{\partial P}\right) + \frac{\alpha_{MnX_4}}{V_{MnX_4}}\left(\frac{\partial V_{MnX_4^{2-}}}{\partial P}\right) + \frac{\alpha_{inter}}{V_{inter}}\left(\frac{\partial V_{inter}}{\partial P}\right) \quad (10)$$

Taking the unit cell volume of $[(CH_3)_4N]_2MnCl_4$, V = 1748 Å^3 (Table 1), the total volume of the organic/inorganic tetrahedra are $V_{N(CH_3)_4} = 8 \times 2.3$ Å^3/org.tet. = 18.4 Å^3 and $V_{MnCl_4} = 4 \times 6.6$ Å^3/inorg.tet. = 26.3 Å^3. In this calculation, we use $V_{Tet} = (8/(9\sqrt{3}))R_{loc}^3$ with R_{N-CH_3} = 1.66 Å and R_{Mn-Cl} = 2.34 Å (refs 9 and 10). Taking values of crystal compressibility, $\kappa([(CH_3)_4N]_2MnCl_4)$ = 0.105 GPa^{-1}, and local compressibilities, $\kappa([CH_3]_4N)$ = 0.0028 GPa^{-1}; $\kappa(MnCl_4)$ = 0.017 GPa^{-1} (Table 2), we deduce a contribution of the molecular tetrahedra to the crystal compressibility of about 0.3%, κ_{intra} = 0.000 29 GPa^{-1}; the remaining 99.7% is due to the intermolecular interactions, κ_{inter} = 0.1047 GPa^{-1}. Therefore, compressibility in these materials is completely governed by intermolecular interactions, whereas the organic/inorganic tetrahedra behave as rigid entities in a pressure range comparable to their bulk modulus. A similar conclusion is obtained for $[(CH_3)_4N]_2MnBr_4$.

CONCLUSIONS

We have determined the crystal compressibility of mixed organic/inorganic $[(CH_3)_4N]_2MnX_4$ crystals and corresponding local compressibilities of the MnX_4 and $(CH_3)_4N$ tetrahedra by correlating XRD, XAS, and Raman spectroscopy data through their equations-of-state. As a salient result, we conclude that these organic/inorganic hybrid crystals have much higher compressibilities (κ > 0.1 GPa^{-1}) than other analogous inorganic chlorides and bromides, which have compressibilites of about 0.03 and 0.05 GPa^{-1}, respectively.[30,33,34] In $[(CH_3)_4N]_2MnX_4$, the local compressibility of the inorganic and organic tetrahedra are much smaller than the crystal compressibility by one and 2 orders of magnitude, respectively. It means that the crystal compressibility is fully governed by the H−X hydrogen bonds keeping the structure of the MnX_4 and $(CH_3)_4N$ tetrahedra as an almost unaltered rigid structure in the low-pressure regime ($P < B_0$).

By applying a local compressibility model to two isostructural crystals, both containing $(CH_3)_4N^+$ cations, we have determined the local compressibility and local Grüneisen parameter of the organic and inorganic tetrahedra. In particular, the knowledge of $\gamma_{loc}(A_1)$ for the totally symmetric tetrahedral stretching mode in MnX_4^{2-} [1.45 (Cl) and 1.15 (Br)] and in $(CH_3)_4N^+$ (3.0) enabled us to obtain the variation of the Mn−X and C−N bond lengths with pressure and, hence, their local EOS. According to this, we can see these relatively soft crystal structures as consisting of rigid interacting tetrahedra that approach each other upon compression from R_{N-Mn} = 5.1 Å to 4.8 Å at 3 GPa in $[(CH_3)_4N]_2MnBr_4$ and from R_{N-Mn} = 5.0 Å[9] to 4.6 Å at 6 GPa in $[(CH_3)_4N]_2MnCl_4$ before crystal decomposition takes place.[7] This critical compression is about 80% in both crystals ($R_{N-Mn} \approx$ 4.6 Å) and leads to disordered structures, the nature of which remains unsolved.

ASSOCIATED CONTENT

Supporting Information

Details of XAS experiments under high-pressure conditions; radiation-induced damage effects; illustrations showing Raman spectra and effects of X-ray irradiation. This material is available free of charge via the Internet at http://pubs.acs.org.

AUTHOR INFORMATION

Corresponding Author

*E-mail: fernando.rodriguez@unican.es.

Notes

The authors declare no competing financial interest.

ACKNOWLEDGMENTS

Financial support from the Spanish Ministerio de Economia y Competitividad (Project No. MAT2012-38664-C02-1), the MALTA−Consolider Ingenio 2010 (Ref No. CSD2007-00045), and a Technical Grant (Ref No. PTA2011-5461-I) are acknowledged. Y.R.L. and L.N. thank the Mobility Program for financial support (Ref No. SB2005-0201) and The University of Cantabria for the postdoctoral fellowship,

respectively. We acknowledge financial support from DIAMOND Synchrotron facility to carry out XRD pressure experiments (Ref No. EE891) and from SOLEIL Synchrotron facility to perform XAS pressure experiments (Ref No. 20130585).

REFERENCES

(1) Gesi, K.; Ozawa, K. *J. Phys. Soc. Jpn.* **1984**, *53*, 627−634.
(2) Gesi, K. *J. Phys. Soc. Jpn.* **1983**, *52*, 2931−2935.
(3) Presser, N.; Ratner, M. A.; Sundheim, B. R. *Chem. Phys.* **1978**, *31*, 281−293.
(4) Zink, J. I.; Hardy, G. E.; Gliemann, G. *Inorg. Chem.* **1980**, *19*, 488−492.
(5) Nikolic, N.; Canny, B.; Curie, D.; Gendrom, F.; Porte, C. *Fizika* **1985**, *17* (1), 27−36.
(6) Cotton, F. A.; Daniels, L. M.; Huang, P. *Inorg. Chem.* **2001**, *40*, 3576−3578.
(7) Rodriguez-Lazcano, Y.; Rodriguez, F.; Nataf, L. *Phys. Rev. B* **2009**, *80*, 085115 (11).
(8) Marco de Lucas, M. C.; Rodriguez, F. *J. Phys.: Condens. Matter* **1993**, *5*, 2625−2642.
(9) Hasebe, K.; Asahi, T. *Acta Crystallogr., Sect. C: Cryst. Struct. Commun.* **1989**, *45*, 841−843.
(10) Mashiyama, H.; Koshiji, N. *Acta Crystallogr., Sect. B* **1989**, *45*, 467−473.
(11) Koshiji, N.; Mashiyama, H. *J. Phys. Soc. Jpn.* **2000**, *69*, 3853−3859.
(12) Perret, R.; Godefroy, G.; Arend, H. *Ferroelectrics* **1987**, *73*, 87−99.
(13) Marco de Lucas, M. C.; Moreno, M.; Rodriguez, F. *Ferroelectrics* **1990**, *109*, 21−26.
(14) Nakamoto, K. *Infrared and Raman Spectra of Inorganic and Coordination Compounds;* Wiley: New York, 1986.
(15) Braudt, M. N.; Couzi, M.; Chanh, N. B.; Gomez-Cuevas, A. *J. Phys.: Condens. Matter* **1990**, *2*, 8229−8242.
(16) Hong, S. B. *Microporous Mater.* **1995**, *4*, 309−317.
(17) Jayasree, R. S.; Nayar, V. U.; Jordanovska, V. *J. Solid State Chem.* **1996**, *127*, 51−55.
(18) Hammersley, A. P.; Svensson, S. O.; Hanfland, M.; Fitch, A. N.; Häusermann, D. *High Pressure Res.* **1996**, *14*, 235−248.
(19) Baudelet, F.; Kong, Q.; Nataf, L.; Cafun, J. D.; Congeduti, A.; Monza, A.; Chagnot, S.; Itié, J. P. *High Pressure Res.* **2011**, *31*, 136−139.
(20) Forman, R. A.; Piermarini, G. J.; Barnett, J. D.; Block, S. *Science* **1972**, *176*, 284−285.
(21) Syassen, K. *High Pressure Res.* **2008**, *28*, 75−126.
(22) Morosin, B.; Graeber, E. J. *Acta Crystallogr.* **1967**, *23*, 766−770.
(23) Alcock, N. W.; Holt, S. L. *Acta Crystallogr., Sect. B* **1978**, *34*, 1970−1972.
(24) Goodyear, J.; Ali, E. M.; Steigmann, G. A. *Acta Crystallogr., Sect. B* **1977**, *33*, 2932−2933.
(25) Goodyear, J.; Ali, E. M.; Sutherland, H. H. *Acta Crystallogr., Sect. B* **1979**, *35*, 456−457.
(26) Hernandez, I.; Rodriguez, F. *J. Phys.: Condens. Matter* **2003**, *15*, 2183−2195.
(27) Murnaghan, F. *Proc. Natl. Acad. Sci. U.S.A.* **1944**, *30*, 244−247.
(28) Ravel, B.; Newville, M. *J. Synchrotron Radiat.* **2005**, *12*, 537−541.
(29) Drickamer; H. G. and Frank; C. W. *Electronic Structure, Electronic Transitions, and the High Pressure Chemistry and Physics of Solids;* Chapman and Hall: London, U.K., 1973.
(30) Aguado, F.; Rodriguez, F.; Lennie, A. R. *J. Phys.: Conf. Ser.* **2010**, *215*, 012009 (4).
(31) Martín-Pendás, A.; Costales, A.; Blanco, M. A.; Recio, J. M.; Luaña, V. *Phys. Rev. B* **2000**, *62*, 13970−13978.
(32) Contreras-García, J.; Mori-Sánchez, P.; Silvi, B.; Recio, J. M. *J. Chem. Theory Comput.* **2009**, *5*, 2108−2114.
(33) Tonkov, Yu. E. *High Pressure Phase Transformations. A Handbook;* Gordon & Breach Science Publisher: Amsterdam, 1992, and references therein.
(34) Aguado, F.; Valiente, R.; Rodriguez, F.; Hanfland, M.; Itié, J. P. *Phys. Rev. B* **2012**, *85*, 100101 (5).